

Control of the radiative level shift and linewidth of a superconducting artificial atom through a variable boundary condition

Kazuki Koshino^{1,4} and Yasunobu Nakamura^{2,3,5}

¹ College of Liberal Arts and Sciences, Tokyo Medical and Dental University, 2-8-30 Konodai, Ichikawa 272-0827, Japan

² Green Innovation Research Laboratories, NEC Corporation, 34 Miyukigaoka, Tsukuba 305-8501, Japan

³ The Institute of Physical and Chemical Research (RIKEN), 2-1 Hirosawa, Wako 351-0198, Japan

E-mail: kazuki.koshino@osamember.org

New Journal of Physics **14** (2012) 043005 (21pp)

Received 6 October 2011

Published 10 April 2012

Online at <http://www.njp.org/>

doi:10.1088/1367-2630/14/4/043005

Abstract. We investigate the dynamics of a superconducting qubit strongly coupled to a semi-infinite one-dimensional microwave field having a variable boundary condition. The radiative level shift and linewidth of the qubit are controllable through the boundary condition of the field, and the spectral properties of the output microwave are modified accordingly. The current scheme provides a compact method for controlling the radiative characteristics of quantum few-level systems that is useful in single-photon engineering.

⁴ Author to whom any correspondence should be addressed.

⁵ Present address: Research Center for Advanced Science and Technology (RCAST), 4-6-1 Komaba, Meguro-ku, Tokyo 153-8904, Japan.

Contents

1. Introduction	2
2. The system	4
2.1. The Hamiltonian	4
2.2. Initial state vector	6
3. Heisenberg equations	6
4. Response of the qubit	8
4.1. Basic equations	8
4.2. Numerical results	8
5. Amplitude of the output field	9
5.1. Linear response	10
6. The power spectrum	11
6.1. Coherent and incoherent components	11
6.2. Fluxes of three components	12
6.3. Spectral shapes of $S_i(\omega)$	13
7. Discussion	15
8. Summary	16
Acknowledgments	16
Appendix A. The boundary condition	16
Appendix B. Derivation of Heisenberg equations	18
Appendix C. Derivation of the power spectrum	19
References	20

1. Introduction

In the early days of quantum mechanics, the transition frequencies and the spontaneous emission rates of atoms were regarded as inherent properties of individual atoms determined by their valence electrons. However, these quantities are sensitive to the dielectric environment such as the spatial profile of the field modes and their density of states, since the optical transitions occur as a result of interaction between the electrons and the light field. When an atom is in a free space, its transition frequencies are shifted slightly through the vacuum fluctuation of the field, which is known as the radiative (Lamb) shift [1, 2]. On the other hand, when an atom is placed in a cavity, its radiative decay can be enhanced or suppressed drastically, which is known as the Purcell effect [3–7]. The changes in the transition frequency and the radiative decay rate are inseparable in general, since they are determined by the real and imaginary parts of the complex frequency of the atom renormalized by interaction with the light field.

In recent years, atoms (including artificial ones) coupled to one-dimensional (1D) photon fields have been realized in a variety of physical systems: trapped atoms [8–13] and molecules [14], quantum dots [15, 16], color centers [17, 18] and superconducting qubits [19–23]. They are classified into two types by their spatial configuration: the direct-coupling type, in which the atom interacts directly with the 1D field [8–11, 14, 15, 17–19], and the cavity quantum electrodynamics (QED) type, in which the atom is coupled with a cavity

mode and then to the propagating field indirectly. The cavity QED systems are further classified by their internal dynamics into the weak-coupling regime [12, 13, 16] and the strong-coupling regime [20–23]. The former (latter) regime is characterized by a shorter (longer) lifetime of a cavity photon than the period of the vacuum Rabi oscillation. The weak-coupling cavity QED systems exhibit essentially the same dynamics as those of the direct-coupling systems, since the degrees of freedom of cavity photons may be eliminated adiabatically [12]. The charm of the strong-coupling cavity QED systems lies in the coherent quantum phenomena played by the atoms and cavity photons, which can be applied to various areas of quantum-state engineering. On the other hand, the charm of the direct-coupling systems lies in their peculiar optical response that originates from inevitable interference between the incident light and the radiation from the atom due to one dimensionality of the field. Recent studies revealed that (i) incident light can be reflected perfectly by a single atom [19, 24], (ii) the nonlinear interaction between single photons can be enhanced drastically [25] and (iii) the Raman-type transitions may become nearly deterministic [26–28].

In this study, we investigate a circuit QED system in which a superconducting qubit is coupled directly to a semi-infinite microwave transmission line and analyze the microwave response of the qubit to stationary pumping. A similar situation was realized by a single ion trapped near a mirror, and the interference of radiation from the ion and its mirror image was confirmed [8, 29]. Compared to this, the current situation has the following three merits in the light of quantum-state engineering. (i) The spontaneous emission into the transmission line overwhelms that into other spatial modes⁶. Therefore, the excitation in the qubit is transformed into a microwave photon nearly perfectly. In other words, the radiation mode of the qubit is matched with the incident wave. (ii) The qubit is motionless and its position can be controlled precisely (typically, 10^{-4} of the wavelength of relevant photons). (iii) The radiative decay rate overwhelms the pure-dephasing rate. Therefore, the radiative decay of the qubit occurs cleanly. In this study, we treat three kinds of dissipation of the qubit (radiative decay, pure dephasing, non-radiative decay) in a non-perturbative manner and observe their interplay.

The physical setup considered here is schematically illustrated in figure 1. The microwave transmission line is terminated by a superconducting quantum interference device (SQUID). This enables us to change the boundary condition at the terminal through the magnetic flux threading the SQUID ring [30–32] and therefore to vary the effective position of the qubit continuously. We theoretically show that the radiative level shift and linewidth of the qubit can be controlled through the boundary condition, and that they are reflected in the properties of the output radiation. This scheme will offer an experimentally compact method for controlling the radiative properties of the qubit and will be useful in future single-photon engineering.

The rest of this paper is organized as follows. The theoretical model is presented in section 2, and the Heisenberg equations are derived in section 3. The microwave response of the qubit is discussed in section 4. The properties of the output microwave radiation, such as the coherent amplitude and the power spectrum, are respectively discussed in sections 5 and 6. The boundary condition of the microwave transmission line is derived for the self-containedness of the paper in appendix A, and the details of the calculation are presented in appendices B and C.

⁶ The ratio between the radiative decay rate into the target mode (Γ_t) and the overall decay rate (Γ_o) can be inferred from the dip in the transmission spectrum. Γ_t/Γ_o is less than 10% in atomic experiments, whereas this value exceeds 90% in circuit QED experiments.

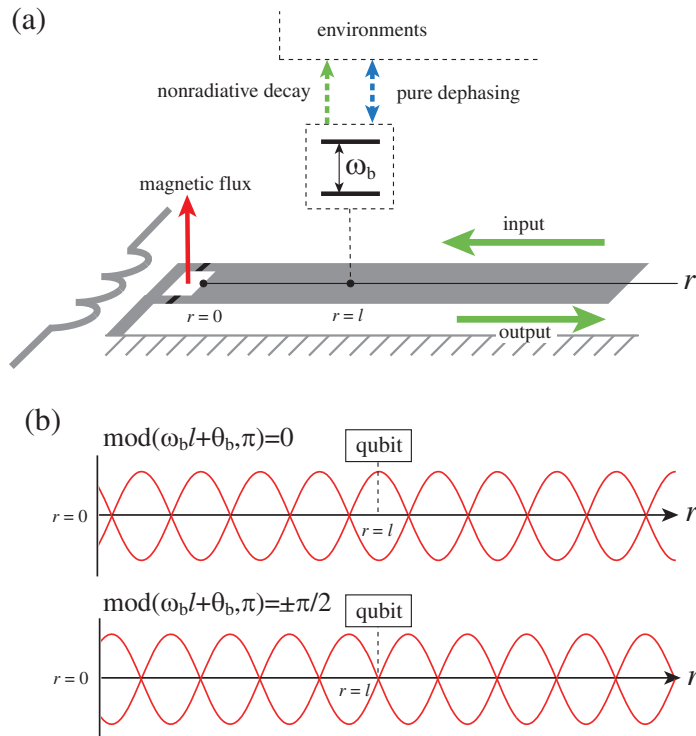


Figure 1. (a) Schematic illustration of the physical setup. A microwave transmission line is terminated by a SQUID ring. The boundary condition can be varied by the amount of magnetic flux threading the ring. A superconducting qubit is coupled to the line at $r = l$. (b) Shape of the microwave eigenmode at the qubit frequency: $\text{mod}(\omega_b l + \theta_b, \pi) / \pi = 0$ and $\pm 1/2$.

2. The system

2.1. The Hamiltonian

The experimental setup considered is illustrated schematically in figure 1. The system is composed of a semi-infinite microwave transmission line terminated by a SQUID ring and a superconducting two-level system (qubit). The transmission line extends in the $r > 0$ region and is terminated at $r = 0$ by the ring, and the qubit is coupled to the line at $r = l$. The eigenmodes of the transmission line in the absence of the qubit are given by

$$f_k(r) = \sqrt{2/\pi} \cos(kr + \theta_b), \quad (1)$$

where k is the wave number and θ_b is the phase shift determined by the magnetic flux threading the ring (see appendix A). We may set $-\pi/2 < \theta_b < \pi/2$ without loss of generality, since $\theta_b + n\pi$ with integer n yields the same mode function as equation (1). Although θ_b is dependent on k rigorously, we can neglect this dependence in the narrow frequency range near the resonance of the qubit. Furthermore, to account for pure dephasing and non-radiative decay induced by environmental degrees of freedom, the qubit is coupled to two independent bosonic reservoirs, both of which are assumed to have the same dispersion relation as the microwave photon for simplicity. Setting $\hbar = v = 1$, where v is the microwave velocity, the Hamiltonian of

the overall system is given by

$$\begin{aligned} \mathcal{H} = & \omega_b \sigma^\dagger \sigma + \int_{-\infty}^{\infty} dk \left[k b_k^\dagger b_k + g_k (\sigma^\dagger b_k + b_k^\dagger \sigma) \right] + \int_{-\infty}^{\infty} dk \left[k c_k^\dagger c_k + h_k \sigma^\dagger \sigma (c_k^\dagger + c_k) \right] \\ & + \int_{-\infty}^{\infty} dk \left[k d_k^\dagger d_k + i_k (\sigma^\dagger d_k + d_k^\dagger \sigma) \right], \end{aligned} \quad (2)$$

where σ is the lowering operator of the qubit, b_k is the annihilation operator of the microwave photon with wave number k and c_k and d_k are the annihilation operators of the reservoir excitations: c_k accounts for pure dephasing and d_k for non-radiative decay. The qubit–photon coupling g_k and the qubit–reservoir couplings h_k and i_k are given by

$$g_k = \sqrt{\Gamma_r/2} f_k(l) = \sqrt{\Gamma_r/\pi} \cos(kl + \theta_b), \quad (3)$$

$$h_k = \sqrt{\Gamma_p/\pi}, \quad (4)$$

$$i_k = \sqrt{\Gamma_n/2\pi}. \quad (5)$$

The meanings of the parameters are as follows. ω_b is the transition frequency of the qubit, and Γ_r , Γ_p and Γ_n , respectively, denote the rates for radiative decay, pure dephasing and non-radiative decay.

For later convenience, we introduce the field operator in the real-space representation. Dividing the eigenmode function of equation (1) into incoming and outgoing components, the input and output field operators are given by $b_{\text{in},r} = (2\pi)^{-1/2} \int_0^\infty dk e^{-i(kr+\theta_b)} b_k$ and $b_{\text{out},r} = (2\pi)^{-1/2} \int_0^\infty dk e^{i(kr+\theta_b)} b_k$, respectively. Since only high-energy excitations ($k \sim \omega_b$) are relevant, we can formally introduce the negative-energy excitations and extend the lower limit of k to $-\infty$. Then we have

$$b_{\text{in},r} = e^{-i\theta_b} \tilde{b}_{-r}, \quad (6)$$

$$b_{\text{out},r} = e^{i\theta_b} \tilde{b}_r, \quad (7)$$

where \tilde{b}_r is the Fourier transform of b_k , as given by

$$\tilde{b}_r = \frac{1}{\sqrt{2\pi}} \int_{-\infty}^{\infty} dk e^{ikr} b_k. \quad (8)$$

Note that the index r in \tilde{b}_r runs over $-\infty < r < \infty$, and the $r < 0$ ($r > 0$) region represents the incoming (outgoing) field. We can formally define \tilde{c}_r and \tilde{d}_r in the same manner.

Several remarks should be made regarding this model. (i) Regarding the b and d fields, high-energy excitations ($k \sim \omega_b$) are relevant in the dynamics. Although negative-energy excitations are introduced in the Hamiltonian, they are highly out of resonance with the qubit and do not affect its microwave response [33]. (ii) In contrast, regarding the c field, low-energy excitations ($k \sim 0$) are relevant, and the generation of negative-energy excitations implies absorption of energy from the environment. h_k would depend not only on the bare interaction strength and the density of states but also on the Boltzmann factor. One may approximately treat h_k as a constant when the energy of relevant excitations is much smaller than the background temperature. This condition is satisfied in circuit QED experiments: since the energy exchange with the c field occurs as a result of inelastic scattering, the relevant energy is determined by the

detuning between the pump photon and the qubit, which is usually of the order of $\Gamma_r \sim 0.5$ mK. In contrast, the background temperature is typically at 50 mK. (iii) When one realizes the setup of figure 1 by using real atoms, the radiative decay into the lateral direction becomes significant [8]. This damping plays the same role as the non-radiative decay employed here. Therefore, the present model can cover the optical cases by interpreting the non-radiative decay as the radiative decay into the lateral direction.

2.2. Initial state vector

In this study, we investigate the microwave response of the qubit to stationary pumping. At the initial moment ($t = 0$), we assume that the qubit is in the ground state, no excitation exists in both reservoirs and the input microwave has not arrived at the qubit. The initial state vector is then written as

$$|\psi_i\rangle = \mathcal{N} \exp\left(\int dr E_{\text{in}}(r) b_{\text{in},r}^\dagger\right) |0\rangle, \quad (9)$$

where $|0\rangle$ is the overall vacuum state and $\mathcal{N} = \exp(-\int dr |E_{\text{in}}(r)|^2/2)$ is a normalization constant. $E_{\text{in}}(r)$ represents the input classical microwave at the initial moment, as given by

$$E_{\text{in}}(r) = \begin{cases} E e^{-i\omega_p r} & (l < r), \\ 0 & (\text{otherwise}), \end{cases} \quad (10)$$

where E and ω_p are the amplitude and frequency of the pump, respectively. Note that $|\psi_i\rangle$ is in a coherent state and is therefore an eigenstate of the initial field operators, satisfying $\tilde{b}_r(0)|\psi_i\rangle = e^{i\theta_b} E_{\text{in}}(-r)|\psi_i\rangle$ and $\tilde{c}_r(0)|\psi_i\rangle = \tilde{d}_r(0)|\psi_i\rangle = 0$. Throughout this paper, we denote $\langle\psi_i|A(t)|\psi_i\rangle$ by $\langle A(t)\rangle$, where A may be any operator.

3. Heisenberg equations

From the Hamiltonian of equation (2), we can rigorously derive the following equations (see appendix B for derivation):

$$\tilde{b}_r(t) = \tilde{b}_{r-t}(0) - ie^{-i\theta_b} \sqrt{\frac{\Gamma_r}{2}} \Theta_{r \in (l, t+l)} \sigma(t-r+l) - ie^{i\theta_b} \sqrt{\frac{\Gamma_r}{2}} \Theta_{r \in (-l, t-l)} \sigma(t-r-l), \quad (11)$$

$$\tilde{c}_r(t) = \tilde{c}_{r-t}(0) - i\sqrt{2\Gamma_p} \Theta_{r \in (0, t)} \sigma^\dagger(t-r) \sigma(t-r), \quad (12)$$

$$\tilde{d}_r(t) = \tilde{d}_{r-t}(0) - i\sqrt{\Gamma_n} \Theta_{r \in (0, t)} \sigma(t-r), \quad (13)$$

$$\begin{aligned} \frac{d}{dt} \sigma = & \left(-i\omega_b - \frac{\Gamma_r + 2\Gamma_p + \Gamma_n}{2} \right) \sigma - \frac{\Gamma_r e^{2i\theta_b}}{2} \Theta_{t \in (2l, \infty)} (1 - 2\sigma^\dagger \sigma) \sigma(t-2l) \\ & - i(1 - 2\sigma^\dagger \sigma) [N_b(t) + N_d(t)] - iN_c^\dagger(t) \sigma - i\sigma N_c(t), \end{aligned} \quad (14)$$

$$\frac{d}{dt} \sigma^\dagger \sigma = \left(-\frac{\Gamma_r + \Gamma_n}{2} \sigma^\dagger \sigma - \frac{\Gamma_r e^{2i\theta_b}}{2} \Theta_{t \in (2l, \infty)} \sigma^\dagger \sigma(t-2l) - i\sigma^\dagger [N_b(t) + N_d(t)] \right) + \text{h.c.}, \quad (15)$$

where

$$\Theta_{r \in (a,b)} = \begin{cases} 1 & (a < r < b), \\ 1/2 & (r = a, b), \\ 0 & (\text{otherwise}), \end{cases} \quad (16)$$

and the noise operators $N_b(t)$, $N_c(t)$ and $N_d(t)$ are defined by

$$N_b(t) = \sqrt{\Gamma_r/2} [e^{i\theta_b} \tilde{b}_{l-t}(0) + e^{-i\theta_b} \tilde{b}_{-l-t}(0)], \quad (17)$$

$$N_c(t) = \sqrt{2\Gamma_p} \tilde{c}_{-t}(0), \quad (18)$$

$$N_d(t) = \sqrt{\Gamma_n} \tilde{d}_{-t}(0). \quad (19)$$

The microwave photons formally propagate only in the positive direction and interact with the qubit at both $r = -l$ and $+l$. This makes the equation of motion of the qubit, equations (14) and (15), non-local in time [29]. However, the position l of the qubit is of the order of the microwave wavelength in the present situation and therefore the dynamics of the qubit is negligible during the short time interval of the order of l/v , except for the natural phase factor. (Typically, $l \sim 1$ cm, $v \sim c/3$, and therefore $l/v \sim 10^{-10}$ s. In contrast, the time scale of the qubit dynamics is determined by $\Gamma_r^{-1} \sim 10^{-8}$ s [19].) We may then safely replace $\sigma(t + \Delta t)$ with $\sigma(t) e^{-i\omega_b \Delta t}$. Furthermore, since we consider the narrow frequency range near resonance, we can also replace $\tilde{b}_{\pm l-t}(0)$ with $e^{\pm i\omega_b l} \tilde{b}_{-t}(0)$. Then, equations (11), (14), (15) and (17) are rewritten as follows:

$$\dot{\tilde{b}}_r(t) = \tilde{b}_{r-t}(0) - i\alpha \tilde{\Gamma}_r^{1/2} \Theta_{r \in (0,t)} \sigma(t-r), \quad (20)$$

$$\frac{d}{dt} \sigma = (-i\tilde{\omega}_b - \Gamma_2) \sigma - i(1 - 2\sigma^\dagger \sigma) [N_b(t) + N_d(t)] - iN_c^\dagger(t) \sigma - i\sigma N_c(t), \quad (21)$$

$$\frac{d}{dt} \sigma^\dagger \sigma = -\Gamma_1 \sigma^\dagger \sigma - i\sigma^\dagger [N_b(t) + N_d(t)] + i[N_b^\dagger(t) + N_d^\dagger(t)] \sigma, \quad (22)$$

$$N_b(t) = \alpha \tilde{\Gamma}_r^{1/2} \tilde{b}_{-t}(0), \quad (23)$$

where $\alpha = \text{sgn}[\cos(\omega_b l + \theta_b)]$, $\tilde{\omega}_b$ and $\tilde{\Gamma}_r$ are the transition frequency and the radiative linewidth of the qubit, which are renormalized by coupling to the semi-infinite field as

$$\tilde{\omega}_b = \omega_b + (\Gamma_r/2) \sin 2(\omega_b l + \theta_b), \quad (24)$$

$$\tilde{\Gamma}_r = 2\Gamma_r \cos^2(\omega_b l + \theta_b), \quad (25)$$

and Γ_1 and Γ_2 are the overall rates for energy relaxation and dephasing, as given by

$$\Gamma_1 = \tilde{\Gamma}_r + \Gamma_n, \quad (26)$$

$$\Gamma_2 = \Gamma_1/2 + \Gamma_p. \quad (27)$$

The commutation relations between the noise and qubit operators are summarized in appendix B. Here, the radiative level shift originates from the coupling to continuous photonic modes as found by Lamb and Retherford [1], in contrast with the shifts originating from the coupling to a discrete cavity mode [23]. Equations (24) and (25) indicate that both the radiative shift and linewidth of the qubit are controllable through the boundary condition. We will observe in the following how these renormalized values are reflected in the microwave response of the qubit.

4. Response of the qubit

4.1. Basic equations

In this section, we observe the response of the qubit to a continuous pump field of equation (10). The equations of motion for $s_1(t) \equiv \langle \sigma(t) \rangle e^{i(\omega_p t - \theta_b)}$ and $s_2(t) \equiv \langle \sigma^\dagger(t) \sigma(t) \rangle$ are given, from equations (9), (21) and (22), by

$$\frac{d}{dt} \begin{pmatrix} s_1 \\ s_1^* \\ s_2 \end{pmatrix} = \begin{pmatrix} -\Gamma_2 + i\delta\omega & 0 & i\alpha\Omega \\ 0 & -\Gamma_2 - i\delta\omega & -i\alpha\Omega \\ i\alpha\Omega/2 & -i\alpha\Omega/2 & -\Gamma_1 \end{pmatrix} \begin{pmatrix} s_1 \\ s_1^* \\ s_2 \end{pmatrix} + \begin{pmatrix} -i\alpha\Omega/2 \\ i\alpha\Omega/2 \\ 0 \end{pmatrix}, \quad (28)$$

where $\delta\omega = \omega_p - \tilde{\omega}_b$ is the detuning between the pump and the renormalized qubit frequency and $\Omega = 2\tilde{\Gamma}_r^{1/2} E$ is the Rabi frequency.

The response of the qubit can be pursued by solving equation (28) with the initial condition of $s_1(0) = s_2(0) = 0$. The transient behavior before reaching the stationary state is determined by the 3×3 matrix appearing in equation (28). When the pump field is resonant ($\delta\omega = 0$), the three eigenvalues of the matrix are given by

$$\lambda = -\Gamma_2, -\frac{\Gamma_1 + \Gamma_2}{2} \pm i\sqrt{\Omega^2 - \left(\frac{\Gamma_1 - \Gamma_2}{2}\right)^2}. \quad (29)$$

Therefore, if the pump field is strong enough to satisfy $\Omega \gg \Gamma_{1,2}$, the upper-state population exhibits oscillatory behavior known as the Rabi oscillation. The qubit reaches its stationary state for $t \gg \Gamma_{1,2}^{-1}$. The stationary values, $\bar{s}_1 = s_1(\infty)$ and $\bar{s}_2 = s_2(\infty)$, are obtained by putting $\frac{d}{dt} = 0$ in equation (28) as

$$\bar{s}_1 = \frac{-i\alpha}{2} \frac{\Gamma_1(\Gamma_2 + i\delta\omega)\Omega}{\Gamma_1|\Gamma_2 + i\delta\omega|^2 + \Gamma_2\Omega^2}, \quad (30)$$

$$\bar{s}_2 = \frac{1}{2} \frac{\Gamma_2\Omega^2}{\Gamma_1|\Gamma_2 + i\delta\omega|^2 + \Gamma_2\Omega^2}. \quad (31)$$

4.2. Numerical results

Transient behavior of s_2 under resonant pumping ($\omega_p = \tilde{\omega}_b$) is shown in figure 2 for several different boundary conditions. The Rabi frequency is given by $\Omega = 2\tilde{\Gamma}_r^{1/2} E$, whereas the damping rate is given by $\Gamma_{1,2} \sim \tilde{\Gamma}_r$, both of which are sensitive to the boundary condition through the renormalization of $\tilde{\Gamma}_r$. The Rabi oscillations can be observed clearly when the Rabi frequency is much larger than the damping rate, namely, $E^2/\Gamma_r \gg \cos^2(\omega_b l + \theta_b)$. This tendency can be confirmed in figure 2.

In order to observe the effects of dissipation, the stationary population \bar{s}_2 of the excited state is plotted as a function of θ_b in figure 3, for several different dissipation rates, Γ_p and Γ_n . It is observed that both dissipative mechanisms decrease the excited state population as expected. Their difference appears in the limit of $\text{mod}(\omega_b l + \theta_b) \rightarrow \pm 0.5\pi$, where the qubit lies at the node of the corresponding eigenmode and therefore cannot be seen by the microwave. \bar{s}_2 is non-vanishing in this limit in the ideal cases of $\Gamma_n = 0$. However, in reality, \bar{s}_2 vanishes in this limit due to finite Γ_n (see the dashed line in figure 3).

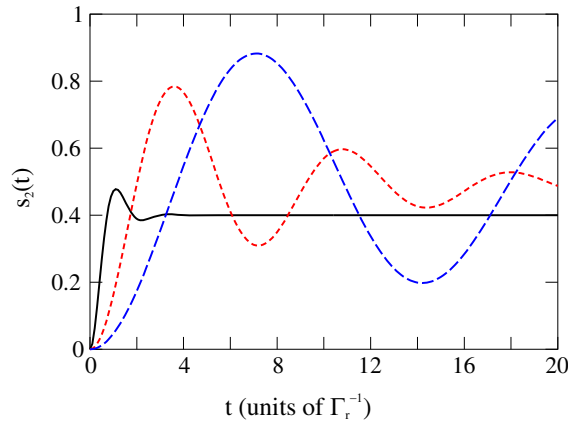


Figure 2. Temporal evolution of the excited state population $s_2(t)$ in the dissipation-free cases ($\Gamma_p = \Gamma_n = 0$) with different boundary conditions: $\text{mod}(\omega_b l + \theta_b, \pi) = 0$ (solid), $\pm 0.4\pi$ (dotted) and $\pm 0.45\pi$ (dashed). The pump is tuned to the renormalized resonance ($\omega_p = \tilde{\omega}_b$) and its intensity is fixed ($E^2 = \Gamma_r$).

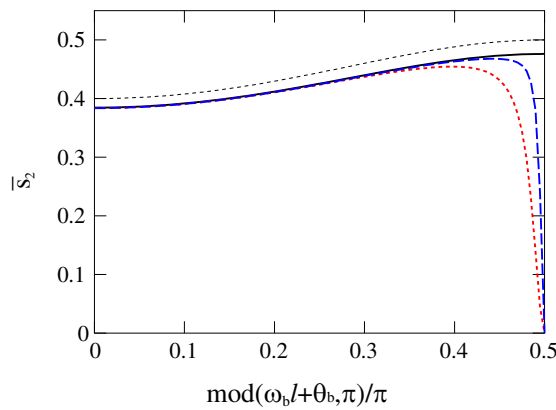


Figure 3. Effects of dissipation on the stationary population \bar{s}_2 of the excited state: no dissipation ($(\Gamma_p, \Gamma_n)/\Gamma_r = (0, 0)$, thin dotted line), pure dephasing ($(\Gamma_p, \Gamma_n)/\Gamma_r = (0.2, 0)$, solid) and non-radiative decay ($(\Gamma_p, \Gamma_n)/\Gamma_r = (0, 0.2)$, dotted). The pump is tuned to the renormalized resonance ($\omega_p = \tilde{\omega}_b$) and its intensity is fixed ($E^2 = \Gamma_r$). Although \bar{s}_2 is non-vanishing at $\text{mod}(\omega_b l + \theta_b, \pi)/\pi = 0.5$ in the ideal cases of $\Gamma_n = 0$, \bar{s}_2 vanishes in reality due to finite Γ_n ($(\Gamma_p, \Gamma_n)/\Gamma_r = (0.2, 0.01)$, dashed line).

5. Amplitude of the output field

In the following sections, we investigate the properties of the output microwave. In this section, we discuss the coherent amplitude of the output wave, $E_{\text{out}}(r, t) = \langle b_{\text{out},r}(t) \rangle$, which can be measured by homodyne-type measurements. From equations (20) and (30), E_{out} is given, in the

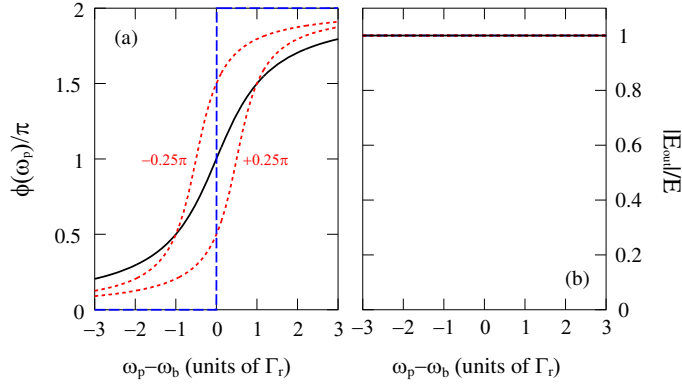


Figure 4. (a) Phase shift and (b) amplitude of the reflected wave, in the linear-response regime ($E^2 \rightarrow 0$) and in the dissipation-free limit ($\Gamma_p = \Gamma_n = 0$). The origin of frequency is set at the *bare* resonance frequency, ω_b . The boundary condition is set at $\text{mod}(\omega_b l + \theta_b, \pi) = 0$ (solid), $\pm 0.25\pi$ (dotted) and $\pm 0.5\pi$ (dashed). Note that the natural phase factor $e^{2i\theta_b}$ is removed in (a) and that all lines are overlapping in (b).

stationary state, by

$$\frac{E_{\text{out}}(r, t)}{E_{\text{in}}(-r, t)} = \left(1 - \frac{\tilde{\Gamma}_r \Gamma_1 (\Gamma_2 + i\delta\omega)}{\Gamma_1 |\Gamma_2 + i\delta\omega|^2 + \Gamma_2 \Omega^2} \right) e^{2i\theta_b}, \quad (32)$$

where $E_{\text{in}}(-r, t) = E e^{i\omega_p(r-t)}$. This expression for E_{out} holds for any input intensity.

5.1. Linear response

The effects of the boundary condition and dissipations are most clearly reflected in the linear response of the qubit. By taking the weak-field limit ($\Omega \rightarrow 0$) in equation (32), the linear response is given by

$$\frac{E_{\text{out}}(r, t)}{E_{\text{in}}(-r, t)} = \frac{2\delta\omega + i(2\Gamma_p + \Gamma_n - \tilde{\Gamma}_r)}{2\delta\omega + i(2\Gamma_p + \Gamma_n + \tilde{\Gamma}_r)} e^{2i\theta_b}. \quad (33)$$

We first discuss the dissipation-free limit of $\Gamma_p = \Gamma_n = 0$. The phase shift $\phi = \arg(E_{\text{out}}/E_{\text{in}})$ and the amplitude $|E_{\text{out}}|$ of the output wave are plotted in figure 4 for several different boundary conditions. (In order to observe the boundary effects clearly, the natural phase factor $e^{2i\theta_b}$ is removed.) We can confirm that $|E_{\text{out}}| = |E_{\text{in}}|$ from equation (33). This implies that the input wave is reflected coherently without attenuation. The input wave is subject to a linear phase shift of $\phi(\omega_p)$, which changes steeply around $\tilde{\omega}_b$ within a narrow frequency width of $\tilde{\Gamma}_r$. Therefore, $\phi(\omega_p)$ is sensitive to the boundary condition as observed in figure 4(a). When $\text{mod}(\omega_b l + \theta_b, \pi) = \pm 0.5\pi$ and therefore $\tilde{\Gamma}_r = 0$, the qubit lies at the node of the corresponding eigenmode. Therefore, the input wave cannot see the qubit and is reflected as it is, $E_{\text{out}} = E_{\text{in}}$.

Next, we discuss the effects of dissipation. Equation (33) implies that, regarding the linear response, the roles of the two dissipative mechanisms, Γ_p and Γ_n , are equivalent. The dissipative version of figure 4 is shown in figure 5. A clear difference from the dissipation-free case is the

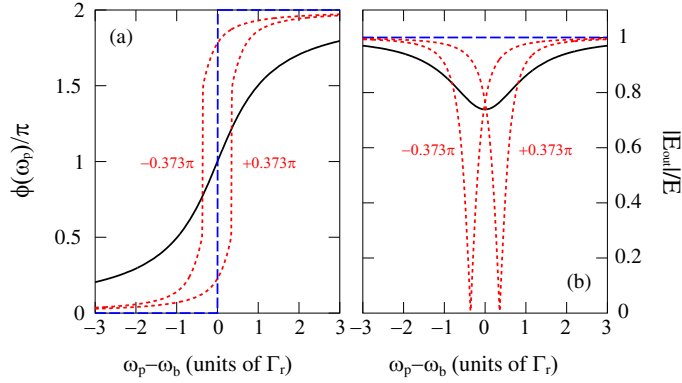


Figure 5. The same plots as figure 4 in the dissipative case ($\Gamma_p + \Gamma_n/2 = 0.15\Gamma_r$). $\text{mod}(\omega_b l + \theta_b, \pi) = 0$ (solid), $\pm 0.373\pi$ (dotted) and $\pm 0.5\pi$ (dashed). $\tilde{\Gamma}_r = 2\Gamma_p + \Gamma_n$ is satisfied for dotted lines.

appearance of a dip in $|E_{\text{out}}(\omega_p)|$, which is located at $\tilde{\omega}_b$ and has a width of $\tilde{\Gamma}_r$. In particular, when $\tilde{\Gamma}_r = 2\Gamma_p + \Gamma_n$ is satisfied (dotted lines in figure 5), the coherent amplitude vanishes in the output port under a resonant pump. In this case, the fate of input photons depends strongly on the nature of dissipation (see section 6.2 for detailed discussion): when pure dephasing is dominant ($\Gamma_p \gg \Gamma_n$), all input photons are reflected into the output port after *inelastic* scattering. In contrast, when non-radiative decay is dominant ($\Gamma_n \gg \Gamma_p$), all input photons are dissipated into environments. This is known as the critical coupling [34].

6. The power spectrum

6.1. Coherent and incoherent components

The power spectrum $S(\omega)$ of the output radiation is defined by

$$S(\omega) = \lim_{T \rightarrow \infty} \int \int_0^T \frac{dt_1 dt_2}{2\pi T} e^{i\omega(t_2 - t_1)} \langle \tilde{b}_r^\dagger(t_1) \tilde{b}_r(t_2) \rangle, \quad (34)$$

where r ($> l$) represents the detector position. Since the correlation function $\langle \tilde{b}_r^\dagger(t_1) \tilde{b}_r(t_2) \rangle$ depends only on $t_1 - t_2$ when stationary, $S(\omega)$ is recast into the following form:

$$S(\omega) = \text{Re} \int_0^\infty \frac{d\tau}{\pi} e^{i\omega\tau} \langle \tilde{b}_r^\dagger(t) \tilde{b}_r(t + \tau) \rangle, \quad (35)$$

where t should satisfy $t \gg r$. $S(\omega)$ can be calculated analytically using the Heisenberg equations (see appendix C for details). It is composed of the coherent and incoherent parts as $S(\omega) = S_c(\omega) + S_i(\omega)$, where

$$S_c(\omega) = |E_{\text{out}}|^2 \delta(\omega - \omega_p), \quad (36)$$

$$S_i(\omega) = (\tilde{\Gamma}_r/\pi) \text{Re} I_3(\omega). \quad (37)$$

E_{out} and $I_3(\omega)$ are given by equations (32) and (C.6).

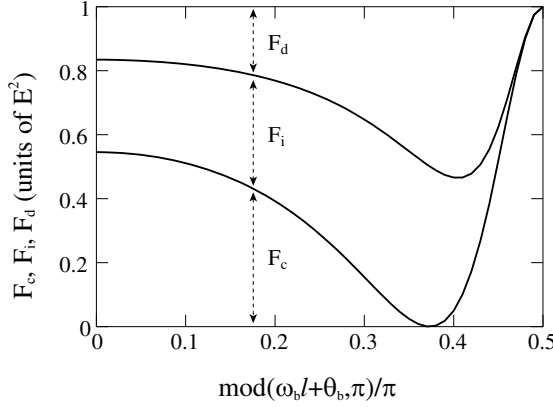


Figure 6. Dependences of F_c , F_i and F_d on the boundary condition. The pump is weak and resonant ($E^2 \rightarrow 0$, $\omega_p = \tilde{\omega}_b$). $\Gamma_p = \Gamma_n = 0.1\Gamma_r$. The coherent component vanishes when $\tilde{\Gamma}_r = \Gamma_n + 2\Gamma_p$.

6.2. Fluxes of three components

The input photons have the following three possibilities after interacting with the qubit, as shown in figure 1: (i) coherent reflection into the output port, (ii) incoherent reflection into the output port and (iii) dissipation into the environment. The photon fluxes for (i) and (ii) are evaluated by $F_c = \int d\omega S_c(\omega)$ and $F_i = \int d\omega S_i(\omega)$. From equations (36) and (C.10), we have

$$F_c = |E_{\text{out}}|^2 = E^2 - \Gamma_1 \bar{s}_2 + \tilde{\Gamma}_r |\bar{s}_1|^2, \quad (38)$$

$$F_i = \tilde{\Gamma}_r (\bar{s}_2 - |\bar{s}_1|^2). \quad (39)$$

The flux for (iii) is defined by $F_d = \int d\omega S_d(\omega)$, where $S_d(\omega)$ is obtained by replacing \tilde{b}_r with \tilde{d}_r in equation (34). It is given by

$$F_d = \langle \tilde{d}_r^\dagger(t) \tilde{d}_r(t) \rangle = \Gamma_n \bar{s}_2. \quad (40)$$

From equations (38)–(40), we have

$$F_c + F_i + F_d = E^2. \quad (41)$$

This represents the flux conservation law, since the input flux is E^2 .

In the linear-response regime ($E^2 \rightarrow 0$), F_i and F_d are reduced to $F_i = \frac{2\Gamma_p \tilde{\Gamma}_r^2}{\Gamma_1 |\Gamma_2 + i\delta\omega|^2} E^2$ and $F_d = \frac{2\Gamma_n \tilde{\Gamma}_r^2 \Gamma_2}{\Gamma_1 |\Gamma_2 + i\delta\omega|^2} E^2$. Figure 6 shows the dependences of F_c , F_i and F_d on the boundary condition, assuming that the pump is always tuned to the renormalized resonance ($\omega_p = \tilde{\omega}_b$). If dissipations are small enough to satisfy $\Gamma_n + 2\Gamma_p < 2\Gamma_r$, one may set the boundary condition to satisfy $\tilde{\Gamma}_r = \Gamma_n + 2\Gamma_p$. Then, the coherent component vanishes in the output, whereas $F_i = \frac{\Gamma_p}{\Gamma_p + \Gamma_n} E^2$ and $F_d = \frac{\Gamma_n}{\Gamma_p + \Gamma_n} E^2$. Therefore, the fate of input photons becomes sensitive to the type of dissipation. When pure dephasing is negligible ($\Gamma_n \gg \Gamma_p$) as in optical experiments, all input photons are dissipated into the environment. This is known as critical coupling [34]. In contrast, when pure dephasing is dominant ($\Gamma_p \gg \Gamma_n$) as in circuit QED experiments, all input photons are reflected back to the output port after *inelastic* scattering. When $\text{mod}(\omega_b l + \theta_b, \pi) = \pm 0.5\pi$ and therefore $\tilde{\Gamma}_r = 0$, the qubit is located at the node of the corresponding eigenmode. Therefore, the pump field cannot see the qubit and is reflected as it is.

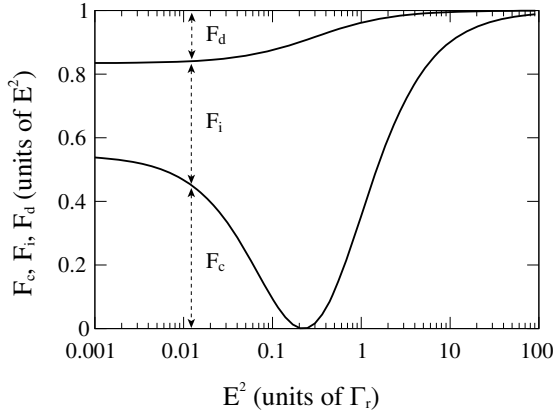


Figure 7. Dependences of F_c , F_i and F_d on the pump intensity E^2 . The boundary condition is fixed at $\text{mod}(\omega_b l + \theta_b, \pi) = 0$ and the pump is resonant ($\omega_p = \tilde{\omega}_b$). The coherent component vanishes when $E^2 = \Gamma_1(\tilde{\Gamma}_r - \Gamma_2)/4\tilde{\Gamma}_r$.

Since equations (38)–(40) are derived non-perturbatively and are valid for any input intensity, we can readily observe the strong field effects. Figure 7 shows the dependences of F_c , F_i and F_d on the input power E^2 , fixing the boundary condition. It is worth noting that, if $\Gamma_n + 2\Gamma_p < \tilde{\Gamma}_r$ is satisfied, the coherent component may vanish at a certain input intensity, $E^2 = \Gamma_1(\tilde{\Gamma}_r - \Gamma_2)/4\tilde{\Gamma}_r$. In the limit of strong pumping ($E^2 \rightarrow \infty$), the qubit becomes saturated ($\bar{s}_2 \rightarrow 1/2$) and does not interact with the field. Therefore, the pump field is reflected as it is in this limit.

6.3. Spectral shapes of $S_i(\omega)$

In the previous subsection, we clarified how the ratios of coherent and incoherent components are determined. Here we investigate the spectral shape of the incoherent component. In the dissipation-free limit ($\Gamma_p = \Gamma_n = 0$), the spectral shape is identical to that of a two-level atom in free space, having the renormalized parameters $\tilde{\omega}_b$ and $\tilde{\Gamma}_r$. Figure 8 shows how the pump intensity E^2 affects the spectral shape. Under a weak pump ($\Omega \lesssim \tilde{\Gamma}_r$), $S_i(\omega)$ has a single peak at the pump frequency ω_p . In contrast, under a strong pump ($\Omega \gtrsim \tilde{\Gamma}_r$), two sidebands appear symmetrically at $\omega_p \pm \Omega$. This is known as the Mollow triplet [19, 35, 36]. As the intensity is increased, the two sidebands shift keeping their linewidths. Figure 9 shows how the boundary condition affects the spectral shape, fixing the pump intensity and frequency. The boundary condition affects the spectrum through renormalization of $\tilde{\Gamma}_r$. The linewidths of the three peaks are proportional to $\tilde{\Gamma}_r$, while the level splitting Ω is proportional to $\tilde{\Gamma}_r^{1/2}$. Therefore, the triplet structure becomes clearer for smaller $\tilde{\Gamma}_r$ [$\text{mod}(\omega_b l + \theta_b, \pi) \rightarrow \pm 0.5\pi$]. This tendency can be confirmed in figure 9.

Next we discuss the effects of dissipation. Here we fix the boundary condition at $\text{mod}(\omega_b l + \theta_b, \pi) = 0$, where $\tilde{\omega}_b = \omega_b$ and $\tilde{\Gamma}_r = 2\Gamma_r$, but qualitatively similar results are obtained for general boundary conditions. Figure 10 shows the effects of dissipation on $S_i(\omega)$ when the pump is tuned to the resonance ($\omega_p = \tilde{\omega}_b$). We can observe that dissipations broaden the peaks, preserving the symmetry of the triplet structure about the pump frequency. The roles of Γ_p and Γ_n are qualitatively the same under resonant pumping. However, the symmetry of

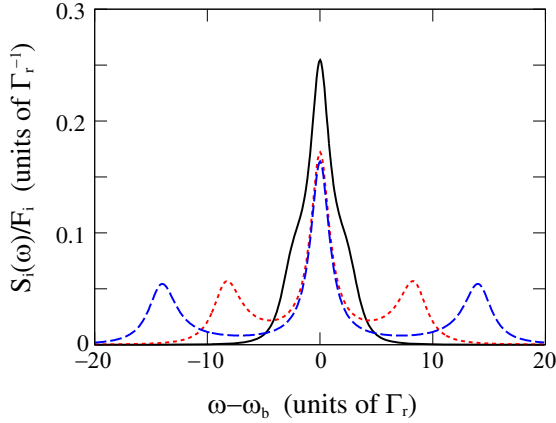


Figure 8. Spectral shapes of $S_i(\omega)$, varying the input intensity: $E^2 = \Gamma_r$ (solid), $9\Gamma_r$ (dotted), $25\Gamma_r$ (dashed). The boundary condition is $\text{mod}(\omega_b l + \theta_b, \pi) = 0$, and the pump is resonant ($\omega_p = \tilde{\omega}_b$). $\Gamma_p = \Gamma_n = 0$.

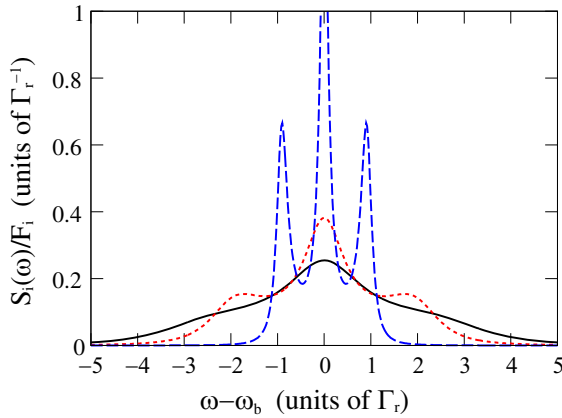


Figure 9. Spectral shapes of $S_i(\omega)$, varying the boundary condition: $\text{mod}(\omega_b l + \theta_b, \pi) = 0$ (solid), $\pm 0.25\pi$ (dotted), $\pm 0.4\pi$ (dashed). $E^2 = \Gamma_r$, $\omega_p = \omega_b$ and $\Gamma_p = \Gamma_n = 0$.

the triplet structure is not necessarily conserved for off-resonant pumping. Figure 11 shows the results when the pump frequency is below the resonance ($\omega_p = \tilde{\omega}_b - 5\Gamma_r$). If pure dephasing is absent ($\Gamma_p = 0$), the symmetry of the spectrum about the pump frequency is preserved. This point is in agreement with the optical results reported in [29] in the Markovian limit. In contrast, if pure dephasing is present ($\Gamma_p > 0$), the symmetry of the spectrum is broken. The sideband closer to the resonance $\tilde{\omega}_b$ becomes larger than the other one. (Although not presented in figure 11, the lower sideband becomes larger than the higher one when $\omega_p > \tilde{\omega}_b$.) Since conservation of photon number is guaranteed by equation (41), asymmetry in the spectrum implies that conservation of photon energy is broken between the input and the output. These facts can be understood as follows. The excitation in the atom is necessarily converted into a single photon in the absence of pure dephasing ($\sigma^\dagger|0\rangle \rightarrow b_k^\dagger|0\rangle$), whereas the atom can emit a photon accompanying low-energy excitations in the environment in the presence of pure dephasing ($\sigma^\dagger|0\rangle \rightarrow b_k^\dagger|0\rangle, b_k^\dagger c_{k'}^\dagger|0\rangle, \dots$). Namely, energy conservation is relaxed by the

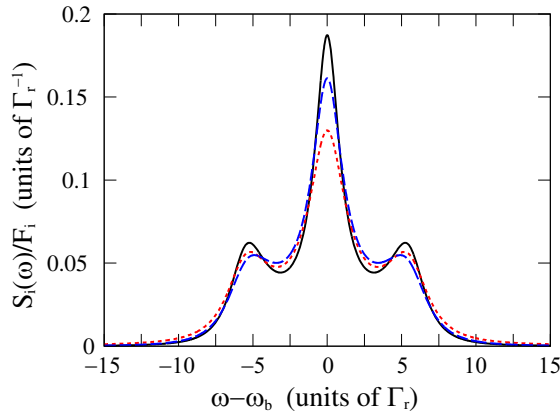


Figure 10. Spectral shapes of $S_i(\omega)$ under resonant pumping ($\omega_p = \omega_b$), for different types of dissipation: $(\Gamma_p, \Gamma_n)/\Gamma_r = (0, 0)$ for solid line, $(0.5, 0)$ for dotted line, and $(0, 0.5)$ for dashed line. $\text{mod}(\omega_b l + \theta_b, \pi) = 0$ and $E^2 = 4\Gamma_r$.

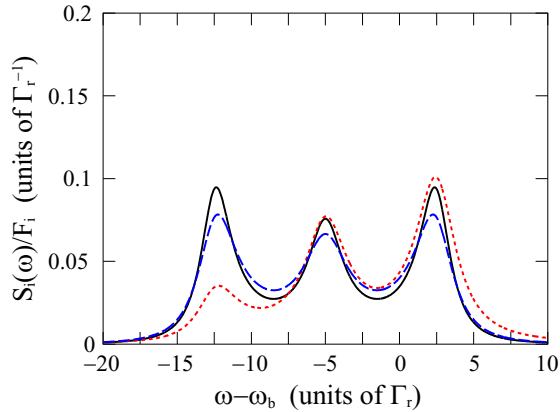


Figure 11. Spectral shapes of $S_i(\omega)$ under off-resonant pumping ($\omega_p = \omega_b - 5\Gamma_r$), for different types of dissipations: $(\Gamma_p, \Gamma_n)/\Gamma_r = (0, 0)$ for solid line, $(0.5, 0)$ for dotted line and $(0, 0.5)$ for dashed line. $\text{mod}(\omega_b l + \theta_b, \pi) = 0$ and $E^2 = 4\Gamma_r$.

pure-dephasing-type interaction with the environment [37]. The atom can then emit photons dominantly near its resonance to break the symmetry.

7. Discussion

We analyzed a superconducting qubit coupled to a semi-infinite transmission line and observed that its transition frequency and linewidth become sensitive to the boundary condition of the line. Since the boundary condition can be varied continuously in circuit QED systems (see appendix A), the current scheme thus provides an experimentally compact method for controlling the radiative property of the qubit. We make two remarks here from the viewpoint of single-photon engineering. (i) The physical origin of the present phenomenon is interference among the following three waves: reflected wave (the first term in equation (11)), radiation

emitted into the positive r -direction (the second term in equation (11)) and radiation emitted into the negative r -direction and reflected afterwards (the third term in equation (11)). Therefore, the conditions for obtaining the present effects by a single photon with pulse length d are as follows: the radiative decay rate is slow enough to satisfy $\Gamma_r \ll v/l$, where v is the microwave velocity in the transmission line, and the pulse length is long enough to satisfy $l \ll d$. Both conditions can be readily satisfied in the circuit QED systems. The giant optical nonlinearity sensitive to individual photons, which is peculiar to such a 1D system, is expected to appear in the present system [25]. (ii) The position dependence of $\tilde{\Gamma}_r$ is determined by its bare transition frequency ω_b (see equation (25)). Therefore, in multi-level quantum systems which have several decay paths with different transition frequencies (Δ -type three-level system, for example [27]), the present scheme will serve as a method for controlling the ratio of radiative decay rates. This would enable us to control the Raman-transition efficiency and would open up a new type of single-photon engineering, which will be discussed elsewhere.

8. Summary

We studied the resonance fluorescence from a superconducting qubit that interacts with a semi-infinite 1D microwave field and is subject to two types of dissipation, pure dephasing and non-radiative damping (figure 1). When coupled to a semi-infinite field, the transition frequency and the radiative linewidth of the qubit are renormalized as equations (24) and (25), and become sensitive to the boundary condition of the field. We analyzed the properties of the output microwave radiation, such as the coherent amplitude and the power spectrum, and observed how the boundary condition and the two types of dissipation modify the properties of output radiation. The present scheme would offer an experimentally compact method for controlling the radiative properties of quantum few-level systems, which would be useful for future single-photon engineering.

Acknowledgments

The authors are grateful to O Astafiev, A A Abdumalikov and T Yamamoto for fruitful discussion. This work was partially supported by the Funding Program for World-Leading Innovative R&D on Science and Technology (FIRST), CREST-JST and MEXT KAKENHI (grant numbers 21102002, 23104710 and 22244035), Strategic Information and Communications R&D Promotion Program (SCOPE no. 111507004) of the Ministry of Internal Affairs and Communications and NICT Commissioned Research.

Appendix A. The boundary condition

For self-containedness of the paper, we briefly overview how the phase θ_b in equation (1) is determined by the magnetic flux threading the SQUID [30]. Figure A.1 shows the effective circuit diagram of a transmission line terminated by a SQUID. The transmission line is modeled by a set of discrete inductances (L) and capacitances (C), and the phase across the j th capacitor is denoted by ϕ_j ($j \geq 1$). The SQUID consists of two identical Josephson junctions (each having capacitance C_s and Josephson energy E_s) forming a loop, and the phases across the junctions are denoted by ϕ_a and ϕ_b . The flux quantization requires that $\phi_a - \phi_b = \phi_{\text{ex}} + 2m\pi$ (m is integer),

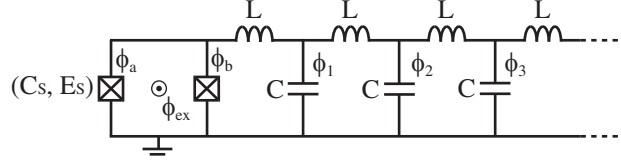


Figure A.1. Equivalent circuit for a transmission line terminated by a SQUID. The transmission line is modeled by a set of discrete inductances and capacitances. The SQUID consists of two identical junctions forming a loop. The external magnetic flux threading the loop is $(\hbar/2e)\phi_{\text{ex}}$.

where $(\hbar/2e)\phi_{\text{ex}}$ is the external magnetic flux threading the loop. The overall Lagrangian is given by

$$\mathcal{L} = \mathcal{L}_{\text{TL}} + \mathcal{L}_{\text{SQ}} + \mathcal{L}_{\text{int}}, \quad (\text{A.1})$$

$$\mathcal{L}_{\text{TL}} = \sum_{j=1}^{\infty} \left(\frac{\hbar}{2e} \right)^2 \left[\frac{C\dot{\phi}_j^2}{2} - \frac{(\phi_{j+1} - \phi_j)^2}{2L} \right], \quad (\text{A.2})$$

$$\mathcal{L}_{\text{SQ}} = \left(\frac{\hbar}{2e} \right)^2 \frac{C_s}{2} (\dot{\phi}_a^2 + \dot{\phi}_b^2) + E_s (\cos \phi_a + \cos \phi_b), \quad (\text{A.3})$$

$$\mathcal{L}_{\text{int}} = - \left(\frac{\hbar}{2e} \right)^2 \frac{(\phi_b - \phi_1)^2}{2L}. \quad (\text{A.4})$$

We switch to new phase variables $\varphi_0 = (\phi_a + \phi_b)/2 + \pi\theta[-\cos(\phi_{\text{ex}}/2)]$ and $\varphi_j = \phi_j + \phi_{\text{ex}}/2 + \pi\theta[-\cos(\phi_{\text{ex}}/2)]$ for $j \geq 1$, where θ is the Heaviside step function. The Lagrangian is then recast in the following form:

$$\mathcal{L}_{\text{TL}} = \sum_{j=1}^{\infty} \left(\frac{\hbar}{2e} \right)^2 \left[\frac{C\dot{\varphi}_j^2}{2} - \frac{(\varphi_{j+1} - \varphi_j)^2}{2L} \right], \quad (\text{A.5})$$

$$\mathcal{L}_{\text{SQ}} = \left(\frac{\hbar}{2e} \right)^2 \frac{\tilde{C}_s}{2} \dot{\varphi}_0^2 + \tilde{E}_s(\phi_{\text{ex}}) \cos \varphi_0, \quad (\text{A.6})$$

$$\mathcal{L}_{\text{int}} = - \left(\frac{\hbar}{2e} \right)^2 \frac{(\varphi_0 - \varphi_1)^2}{2L}, \quad (\text{A.7})$$

where $\tilde{C}_s = 2C_s$ and $\tilde{E}_s(\phi_{\text{ex}}) = 2E_s|\cos(\phi_{\text{ex}}/2)|$. Therefore, the SQUID works as a single Josephson junction having a tunable Josephson energy $\tilde{E}_s(\phi_{\text{ex}})$ through the external magnetic flux ϕ_{ex} .

The equations of motion for φ_0 and φ_j ($j \geq 1$) are, respectively, given by

$$\tilde{C}_s \ddot{\varphi}_0 = -(2e/\hbar)^2 \tilde{E}_s(\phi_{\text{ex}}) \sin \varphi_0 + (\varphi_1 - \varphi_0)/L, \quad (\text{A.8})$$

$$C \ddot{\varphi}_j = -(2\varphi_j - \varphi_{j-1} - \varphi_{j+1})/L. \quad (\text{A.9})$$

We hereafter treat the phase variable as a continuous one $\varphi(r, t)$, which is related to $\varphi_j(t)$ by $\varphi_j(t) = \varphi(j\Delta x, t)$, where Δx is the distance between the neighboring inductances. We also

introduce the inductance and capacitance per unit length by $L_0 = L/\Delta x$ and $C_0 = C/\Delta x$. Equation (A.9) is then reduced to the wave equation

$$\frac{\partial^2 \varphi}{\partial t^2} = v^2 \frac{\partial^2 \varphi}{\partial r^2}, \quad (\text{A.10})$$

where $v = (L_0 C_0)^{-1/2}$ is the velocity of the microwave. On the other hand, equation (A.8) is recast in the following form after linearization:

$$\tilde{C}_s \ddot{\varphi}(0, t) = - \left(\frac{2e}{\hbar} \right)^2 \tilde{E}_s(\phi_{\text{ex}}) \varphi(0, t) + \frac{1}{L_0} \frac{\partial \varphi}{\partial r}(0, t), \quad (\text{A.11})$$

which determines the boundary condition at $r = 0$.

The eigenmode function at the resonance frequency is given by $\varphi(r, t) = f_{\omega_b/v}(r) e^{-i\omega_b t}$, where $f_k(r)$ is given by equation (1). Substituting this into equation (A.11), we obtain the equation that determines θ_b as a function of the external magnetic flux ϕ_{ex} :

$$\tan \theta_b = \frac{2Z_0}{\omega_b} \left[\omega_b^2 C_s - \left(\frac{2e}{\hbar} \right)^2 E_s |\cos(\phi_{\text{ex}}/2)| \right], \quad (\text{A.12})$$

where $Z_0 = \sqrt{L_0/C_0}$ is the characteristic impedance of the transmission line. Typically, $Z_0 \sim 50 \Omega$, $\omega_b \sim 10 \text{ GHz}$, $C_s \sim 100 \text{ fF}$ and $(2e/\hbar)E_s \sim 5 \mu\text{A}$. Therefore, we may vary θ_b largely through the external magnetic flux ϕ_{ex} .

Appendix B. Derivation of Heisenberg equations

We first derive the input–output relation, equation (11), for the microwave photon field. From the Hamiltonian of equation (2), the Heisenberg equations for b_k are given by

$$\frac{d}{dt} b_k = -ikb_k - i\sqrt{\frac{\Gamma_r}{4\pi}} (e^{ikl+i\theta_b} + e^{-ikl-i\theta_b}) \sigma. \quad (\text{B.1})$$

For $0 < t$, this equation can be formally solved as

$$b_k(t) = b_k(0) e^{-ikt} - ie^{-i\theta_b} \sqrt{\frac{\Gamma_r}{4\pi}} \int_0^t d\tau \sigma(\tau) e^{ik(\tau-t-l)} - ie^{i\theta_b} \sqrt{\frac{\Gamma_r}{4\pi}} \int_0^t d\tau \sigma(\tau) e^{ik(\tau-t+l)}. \quad (\text{B.2})$$

Switching to the real-space representation by equation (8), we obtain the following input–output relation for photons:

$$\tilde{b}_r(t) = \tilde{b}_{r-t}(0) - ie^{-i\theta_b} \sqrt{\frac{\Gamma_r}{2}} \Theta_{r \in (l, t+l)} \sigma(t-r+l) - ie^{i\theta_b} \sqrt{\frac{\Gamma_r}{2}} \Theta_{r \in (-l, t-l)} \sigma(t-r-l), \quad (\text{B.3})$$

where $\Theta_{r \in (a, b)}$ is defined by equation (16). Similarly, $\tilde{c}_r(t)$ and $\tilde{d}_r(t)$ are given by

$$\tilde{c}_r(t) = \tilde{c}_{r-t}(0) - i\sqrt{2\Gamma_p} \Theta_{r \in (0, t)} \sigma^\dagger(t-r) \sigma(t-r), \quad (\text{B.4})$$

$$\tilde{d}_r(t) = \tilde{d}_{r-t}(0) - i\sqrt{\Gamma_n} \Theta_{r \in (0, t)} \sigma(t-r). \quad (\text{B.5})$$

The Heisenberg equations for σ and $\sigma^\dagger \sigma$ are given, from equation (2), by

$$\frac{d}{dt} \sigma = -i\omega_b \sigma - i\sqrt{\frac{\Gamma_r}{2}} (1 - 2\sigma^\dagger \sigma) (e^{i\theta_b} \tilde{b}_l + e^{-i\theta_b} \tilde{b}_{-l}) - i\sqrt{2\Gamma_p} \sigma (\tilde{c}_0^\dagger + \tilde{c}_0) - i\sqrt{\Gamma_n} (1 - 2\sigma^\dagger \sigma) \tilde{d}_0, \quad (\text{B.6})$$

$$\frac{d}{dt}\sigma^\dagger\sigma = -i\sigma^\dagger \left[\sqrt{\frac{\Gamma_r}{2}}(e^{i\theta_b}\tilde{b}_l + e^{-i\theta_b}\tilde{b}_{-l}) + \sqrt{\Gamma_n}\tilde{d}_0 \right] + \text{h.c.} \quad (\text{B.7})$$

Using equations (17)–(19), the above equations are recast as equations (14) and (15).

The commutation relations between the noise operators and the atomic operator are derived as follows. Putting $r = t - t'$ in equation (B.5) and using the equal-time commutation relation, $[\tilde{d}_{t-t'}(t), S(t)] = 0$, where S may be any atomic operator, we obtain

$$[N_d(t'), S(t)] = i\Gamma_n \Theta_{t' \in (0,t)} [\sigma(t'), S(t)]. \quad (\text{B.8})$$

Similarly, we have

$$[N_b(t'), S(t)] = i\tilde{\Gamma}_r \Theta_{t' \in (0,t)} [\sigma(t'), S(t)], \quad (\text{B.9})$$

$$[N_c(t'), S(t)] = 2i\Gamma_p \Theta_{t' \in (0,t)} [\sigma^\dagger(t')\sigma(t'), S(t)]. \quad (\text{B.10})$$

Appendix C. Derivation of the power spectrum

Here we derive the analytic form of $S(\omega)$ based on equation (35). For notational simplicity, we set $r \rightarrow +0$ in this section. From equation (20), the two-time correlation function of the field is composed of four terms as

$$\begin{aligned} \langle \tilde{b}_0^\dagger(t)\tilde{b}_0(t+\tau) \rangle &= \langle \tilde{b}_{-t}(0) \rangle^* \langle \tilde{b}_{-t-\tau}(0) \rangle + i\alpha\tilde{\Gamma}_r^{1/2} \langle \sigma(t) \rangle^* \langle \tilde{b}_{-t-\tau}(0) \rangle \\ &\quad - i\alpha\tilde{\Gamma}_r^{1/2} \langle \tilde{b}_{-t}(0) \rangle^* \langle \sigma(t+\tau) \rangle + \tilde{\Gamma}_r \langle \sigma^\dagger(t)\sigma(t+\tau) \rangle, \end{aligned} \quad (\text{C.1})$$

where we have used the fact that $|\psi_i\rangle$ is an eigenstate of $\tilde{b}_r(0)$. The first three terms contribute to the coherent part of the spectrum,

$$S^{(1+2+3)}(\omega) = (E^2 - \Gamma_1\bar{s}_2)\delta(\omega - \omega_p). \quad (\text{C.2})$$

In order to determine the two-time correlation function of the atom, we define the following three quantities: $s_3(\tau) = \langle \sigma^\dagger(t)\sigma(t+\tau) \rangle e^{i\omega_p\tau}$, $s_4(\tau) = \langle \sigma^\dagger(t)\sigma^\dagger(t+\tau) \rangle e^{-i\omega_p(2t+\tau)}$, $s_5(\tau) = \langle \sigma^\dagger(t)\sigma^\dagger(t+\tau)\sigma(t+\tau) \rangle e^{-i\omega_p t}$, all of which are independent of t when stationary. The equations of motion for these quantities are given, from equations (21), (22) and (B.8)–(B.10), by

$$\frac{d}{d\tau} \begin{pmatrix} s_3 \\ s_4 \\ s_5 \end{pmatrix} = \begin{pmatrix} -\Gamma_2 + i\delta\omega & 0 & i\alpha\Omega \\ 0 & -\Gamma_2 - i\delta\omega & -i\alpha\Omega \\ i\alpha\Omega/2 & -i\alpha\Omega/2 & -\Gamma_1 \end{pmatrix} \begin{pmatrix} s_3 \\ s_4 \\ s_5 \end{pmatrix} + \begin{pmatrix} -i\alpha\Omega\bar{s}_1^*/2 \\ i\alpha\Omega\bar{s}_1^*/2 \\ 0 \end{pmatrix}, \quad (\text{C.3})$$

with the initial conditions of $s_3(0) = \bar{s}_2$ and $s_4(0) = s_5(0) = 0$. Since the two-time correlation functions factor in the $\tau \rightarrow \infty$ limit, the stationary values are given by $\bar{s}_3 = |\bar{s}_1|^2$, $\bar{s}_4 = (\bar{s}_1^*)^2$, $\bar{s}_5 = \bar{s}_1^*\bar{s}_2$. Using new variables $\delta s_j(\tau) = s_j(\tau) - \bar{s}_j$ ($j = 3, 4, 5$), the above equations are rewritten as

$$\frac{d}{d\tau} \begin{pmatrix} \delta s_3 \\ \delta s_4 \\ \delta s_5 \end{pmatrix} = \begin{pmatrix} -\Gamma_2 + i\delta\omega & 0 & i\alpha\Omega \\ 0 & -\Gamma_2 - i\delta\omega & -i\alpha\Omega \\ i\alpha\Omega/2 & -i\alpha\Omega/2 & -\Gamma_1 \end{pmatrix} \begin{pmatrix} \delta s_3 \\ \delta s_4 \\ \delta s_5 \end{pmatrix}, \quad (\text{C.4})$$

with the initial conditions of $\delta s_3(0) = \bar{s}_2 - |\bar{s}_1|^2$, $\delta s_4(0) = -(\bar{s}_1^*)^2$, $\delta s_5(0) = -\bar{s}_1^* \bar{s}_2$. We denote the Fourier transforms of $\delta s_j(\tau)$ by $I_j(\omega) = \int_0^\infty d\tau e^{i(\omega - \omega_p)\tau} \delta s_j(\tau)$. After partial integration, they are given by

$$\begin{pmatrix} I_3 \\ I_4 \\ I_5 \end{pmatrix} = \begin{pmatrix} \mu_1 & 0 & i\alpha\Omega \\ 0 & \mu_2 & -i\alpha\Omega \\ i\alpha\Omega^*/2 & -i\alpha\Omega/2 & \mu_3 \end{pmatrix}^{-1} \begin{pmatrix} |\bar{s}_1|^2 - \bar{s}_2 \\ (\bar{s}_1^*)^2 \\ \bar{s}_1^* \bar{s}_2 \end{pmatrix}, \quad (\text{C.5})$$

where $\mu_1 = -\Gamma_2 + i(\omega - \tilde{\omega}_b)$, $\mu_2 = -\Gamma_2 + i(\omega + \tilde{\omega}_b - 2\omega_p)$ and $\mu_3 = -\Gamma_1 + i(\omega - \omega_p)$. Therefore, $I_3(\omega)$ is given by

$$I_3(\omega) = \frac{|\bar{s}_1|^2 - \bar{s}_2}{\mu_1} + \frac{\Omega^2(\bar{s}_1^*)^2 - \Omega^2(|\bar{s}_1|^2 - \bar{s}_2)\mu_2/\mu_1 - 2i\alpha\Omega\bar{s}_1^*\bar{s}_2\mu_2}{2\mu_1\mu_2\mu_3 + \Omega^2(\mu_1 + \mu_2)}. \quad (\text{C.6})$$

Combining the above results, the fourth term in the right-hand side of equation (C.1) contributes to both coherent and incoherent parts of the spectrum,

$$S^{(4)}(\omega) = \tilde{\Gamma}_r |\bar{s}_1|^2 \delta(\omega - \omega_p) + \frac{\tilde{\Gamma}_r}{2\pi} [I_3(\omega) + \text{c.c.}]. \quad (\text{C.7})$$

From equations (C.2) and (C.7), the power spectrum is given by $S(\omega) = S_c(\omega) + S_i(\omega)$, where the coherent and incoherent components are given by

$$S_c(\omega) = |E_{\text{out}}|^2 \delta(\omega - \omega_p), \quad (\text{C.8})$$

$$S_i(\omega) = \frac{\tilde{\Gamma}_r}{2\pi} [I_3(\omega) + \text{c.c.}], \quad (\text{C.9})$$

where E_{out} is given by equation (32), and $|E_{\text{out}}|^2 = E^2 - \Gamma_1 \bar{s}_2 + \tilde{\Gamma}_r |\bar{s}_1|^2$. By the definition of $I_3(\omega)$, we have

$$\int d\omega S_i(\omega) = \tilde{\Gamma}_r (\bar{s}_2 - |\bar{s}_1|^2). \quad (\text{C.10})$$

References

- [1] Lamb W E and Retherford R C 1947 *Phys. Rev.* **72** 241
- [2] Scully M O and Zubairy M S 1997 *Quantum Optics* (Cambridge: Cambridge University Press)
- [3] Purcell E M 1946 *Phys. Rev.* **69** 681
- [4] Yablonovitch E 1987 *Phys. Rev. Lett.* **58** 2059
- [5] Lodahl P, van Driel A F, Nikolaev I S, Irman A, Overgaag K, Vanmaekelbergh D and Vos W L 2004 *Nature* **430** 654
- [6] Kress A, Hofbauer F, Reinelt N, Kaniber M, Krenner H J, Meyer R, Bohm G and Finley J J 2005 *Phys. Rev. B* **71** 241304
- [7] Englund D, Fattal D, Waks E, Solomon G, Zhang B, Nakaoka T, Arakawa Y, Yamamoto Y and Vuckovic J 2005 *Phys. Rev. Lett.* **95** 013904
- [8] Eschner J, Raab C, Schmidt-Kaler F and Blatt R 2001 *Nature* **413** 495
- [9] Wilson M A, Bushev P, Eschner J, Schmidt-Kaler F, Becher C and Blatt R 2003 *Phys. Rev. Lett.* **91** 213602
- [10] Tey M K, Chen Z, Aljunid S A, Chng B, Huber F, Maslennikov G and Kurtsiefer C 2008 *Nature Phys.* **4** 924
- [11] Hétet G, Slodicka L, Hennrich M and Blatt R 2011 *Phys. Rev. Lett.* **107** 133002
- [12] Turchette Q A, Hood C J, Lange W, Mabuchi H and Kimble H J 1995 *Phys. Rev. Lett.* **75** 4710

- [13] Aoki T, Parkins A S, Alton D J, Regal C A, Dayan B, Ostby E, Vahala K J and Kimble H J 2009 *Phys. Rev. Lett.* **102** 083601
- [14] Gerhardt I, Wrigge G, Bushev P, Zumofen G, Agio M, Pfab R and Sandoghdar V 2007 *Phys. Rev. Lett.* **98** 033601
- [15] Vamivakas A N, Atature M, Dreiser J, Yilmaz S T, Badolato A, Swan A K, Goldberg B B, Imamolu A and Unlu M S *Nano Lett.* **7** 2892
- [16] Fushman I, Englund D, Faraon A, Stoltz N, Petroff P and Vuckovic J 2008 *Science* **320** 769
- [17] Babinec T M, Hausmann B J M, Khan M, Zhang Y, Maze J R, Hemmer P R and Loncar M 2010 *Nature Nanotechnol.* **5** 195
- [18] Castelletto S *et al* 2011 *New J. Phys.* **13** 025020
- [19] Astafiev O, Zagoskin A M, Abdumalikov A A, Pashkin Y A, Yamamoto T, Inomata K, Nakamura Y and Tsai J S 2010 *Science* **327** 840
- [20] Blais A, Huang R S, Wallraff A, Girvin S M and Schoelkopf R J 2004 *Phys. Rev. A* **69** 062320
- [21] Wallraff A, Schuster D I, Blais A, Frunzio L, Huang R S, Majer J, Kumar S, Girvin S M and Schoelkopf R J 2004 *Nature* **431** 162
- [22] Bishop L S, Chow J M, Koch J, Houck A A, Devoret M H, Thuneberg E, Girvin S M and Schoelkopf R J 2008 *Nature Phys.* **5** 105
- [23] Fregner A, Goppl M, Fink J M, Baur M, Bianchetti R, Leek P J, Blais A and Wallraff A 2008 *Science* **322** 1357
- [24] Shen J T and Fan S 2005 *Phys. Rev. Lett.* **95** 213001
- [25] Zheng H, Gauthier D J and Baranger H U 2010 *Phys. Rev. A* **82** 063816
- [26] Chang D E, Sorensen A S, Demler E A and Lukin M D 2007 *Nature Phys.* **3** 807
- [27] Koshino K 2009 *Phys. Rev. A* **79** 013804
- [28] Koshino K, Ishizaka S and Nakamura Y 2010 *Phys. Rev. A* **82** 010301
- [29] Dorner U and Zoller P 2002 *Phys. Rev. A* **66** 023816
- [30] Wallquist M, Shumeiko V S and Wendin G 2006 *Phys. Rev. B* **74** 224506
- [31] Yamamoto T, Inomata K, Watanabe M, Matsuba K, Miyazaki T, Oliver W D, Nakamura Y and Tsai J S 2008 *Appl. Phys. Lett.* **93** 042510
- [32] Johansson J R, Johansson G, Wilson C M and Nori F 2009 *Phys. Rev. Lett.* **103** 147003
- [33] Walls D F and Milburn G J 1995 *Quantum Optics* (New York: Springer)
- [34] Cai M, Painter O and Vahala K J 2000 *Phys. Rev. Lett.* **85** 74
- [35] Mollow B R 1969 *Phys. Rev.* **188** 1969
- [36] Wu F Y, Grove R E and Ezekiel S 1975 *Phys. Rev. Lett.* **35** 1426
- [37] Koshino K 2011 *Phys. Rev. A* **84** 033824